Gaussian curvature directs the distribution of spontaneous curvature on bilayer membrane necks

Morgan Chabanon[1] **and Padmini Rangamani**[1,*]

[1]Department of Mechanical and Aerospace Engineering, University of California San Diego, La Jolla, CA, USA.
[*]padmini.rangamani@eng.ucsd.edu

ABSTRACT

Formation of membrane necks is crucial for fission and fusion. In this work, we aim to answer the following fundamental question: what is the relationship between spontaneous curvature and the Gaussian curvature at a membrane neck? We use the Helfrich model for lipid bilayers and solve the shape equation on catenoids to find the field of spontaneous curvature that will stabilize the membrane neck. In this case, the shape equation reduces to a variable coefficient Helmholtz equation for spontaneous curvature, where the source term is proportional to the Gaussian curvature. We show how this latter quantity is responsible for non-uniform distribution of spontaneous curvature in minimal surfaces. We then explore the energetics of catenoids with different spontaneous curvature boundary conditions and geometric asymmetries to show how heterogeneities in spontaneous curvature distribution can couple with Gaussian curvature to result in membrane necks of different geometries.

Introduction

Neck-like structures are a necessary geometric intermediate for fusion and fission in cellular membranes and play important roles in membrane trafficking (both in endo- and exocytosis) and transport within the endomembrane system[1–4]. Furthermore, the formation of necks is a critical step in the interaction of toxins and viral fusion proteins with cellular membranes[5–8]. These structures are also observed in synthetic membrane systems such as in giant unilamellar vesicles subject to osmotic stress[9,10], lipid heterogeneities[11,12], protein insertion or crowding[13,14], and membrane-substrate interactions[15]. As shown in Fig. 1(a), the mechanisms producing neck structures are as diverse as the underlying biological processes. Despite this diversity, their formation is subject to similar biophysical constraints, and most often requires bending the membrane in the presence of compositional in-plane heterogeneities. These membranes heterogeneities can be produced in many ways, resulting in a preferred curvature known as the spontaneous curvature[16–20]. The mechanisms inducing spontaneous curvature on the membrane can broadly be classified into five categories: lipid asymmetry across the leaflets, hydrophobic insertion due to proteins, scaffolding due to proteins, oligomerization, and crowding due to proteins or other external moieties. The local value of spontaneous curvature that influences the formation of neck-like structures can then be interpreted as the combined result of several of these mechanisms.

Despite the wide variety of neck formation mechanisms, some unifying features of membrane necks can be identified. Geometrically, necks are characterized by having a saddle splay shape at every point (see Fig. 1(b)). This is expressed mathematically by a negative Gaussian curvature (two principal curvatures of opposite sign) everywhere on their surface. Most often, necks are assumed to adopt a catenoid-like geometry[21–24]. Although this assumption may appear simplistic, it has been shown helpful in the understanding of biophysical principles of neck formation[21–24]. Catenoids are minimal surfaces; they minimize the surface energy subject to the boundary conditions and have negative Gaussian curvature everywhere, which is required for the formation of neck[7].

In this work, we seek to understand how spontaneous curvature interacts with the Gaussian curvature of catenoid-shaped membrane necks. At the continuum scale, the energy of a lipid bilayer is commonly described by the Helfrich energy[18,25–27]. This model and its extensions relate the bending energy of a lipid membrane to its mean, spontaneous, and Gaussian curvatures. In most studies, the contribution of the Gaussian curvature is not significant because of the

NOTATIONS

A	Area of the catenoid
C	Spontaneous curvature
C_0	Spontaneous curvature at the lower boundary of the catenoid
C_1	Spontaneous curvature at the upper boundary of the catenoid when different from C_0
H	Mean curvature
H_0	Height of the catenoid
K	Gaussian curvature
k	Bending modulus
k_G	Gaussian modulus
L	Total arclength of the symmetric catenoid
l_0	Length truncated from the total arclength in the asymmetric catenoid
λ	Surface tension (Lagrange multiplier)
λ_0	Reference surface tension
p	Pressure difference across the membrane (Lagrange multiplier)
r	Radial coordinate in axisymmetry
r_n	Neck radius of the catenoid
s	Arclength variable of the catenoid
T	Oscillator period (Appendix)
T^*	Critical oscillator period (Appendix)
θ^α	Surface coordinates ($\alpha = 1,2$)
W	Energy of the membrane
w	Energy of the membrane per unit area
ω	Angular frequency of the harmonic oscillator (Appendix)
ω^*	Critical angular frequency of the harmonic oscillator (Appendix)
z	Axial coordinate in axisymmetry

Gauss-Bonnet theorem[28,29], which states that the integral of the Gaussian curvature over a surface only depends on the variations of the boundaries and topology of this surface. While this certainly means that the Gaussian curvature will not influence the energy of a system with fixed or no boundaries such as a closed vesicle, this is not the case, in general, for open boundaries or necks. Particularly, in the case of minimal surfaces such as catenoids where the mean curvature is zero, the Gaussian curvature is the only contribution of the curvature tensor to the energy, and therefore plays a critical role in the determination of the equilibrium state of the system.

Motivated by these considerations, we ask the following questions: Given a catenoid-shaped neck, what is the spontaneous curvature field on this surface that minimizes the Helfrich energy? How is this spontaneous curvature field influenced by the neck radius? And finally, how can we modulate the field of spontaneous curvature in order to promote the necking process? To answer these questions, we use the classical Helfrich theory[25] and conduct simulations to identify how the Gaussian curvature and the spontaneous curvature are related in catenoid-shaped necks.

Methods

Model development. In this section we briefly summarize the Helfrich theory of lipid bilayer and apply it to catenoids. The Helfrich model is valid for deformations of the membrane that are much larger than the thickness of the bilayer[25,26]. In line with previous models[18,30,31], we assume that the membrane is a purely elastic material, ignoring the viscous contributions and the diffusion of proteins within the bilayer. Lipid bilayers are characterized by a high stretching modulus[32]; therefore we represent the membrane as an incompressible surface and use a Lagrange multiplier to implement this constraint. Finally we assume that the asymmetry across the bilayer can be represented by a spontaneous curvature that locally captures the heterogeneity across the membrane[17–19].

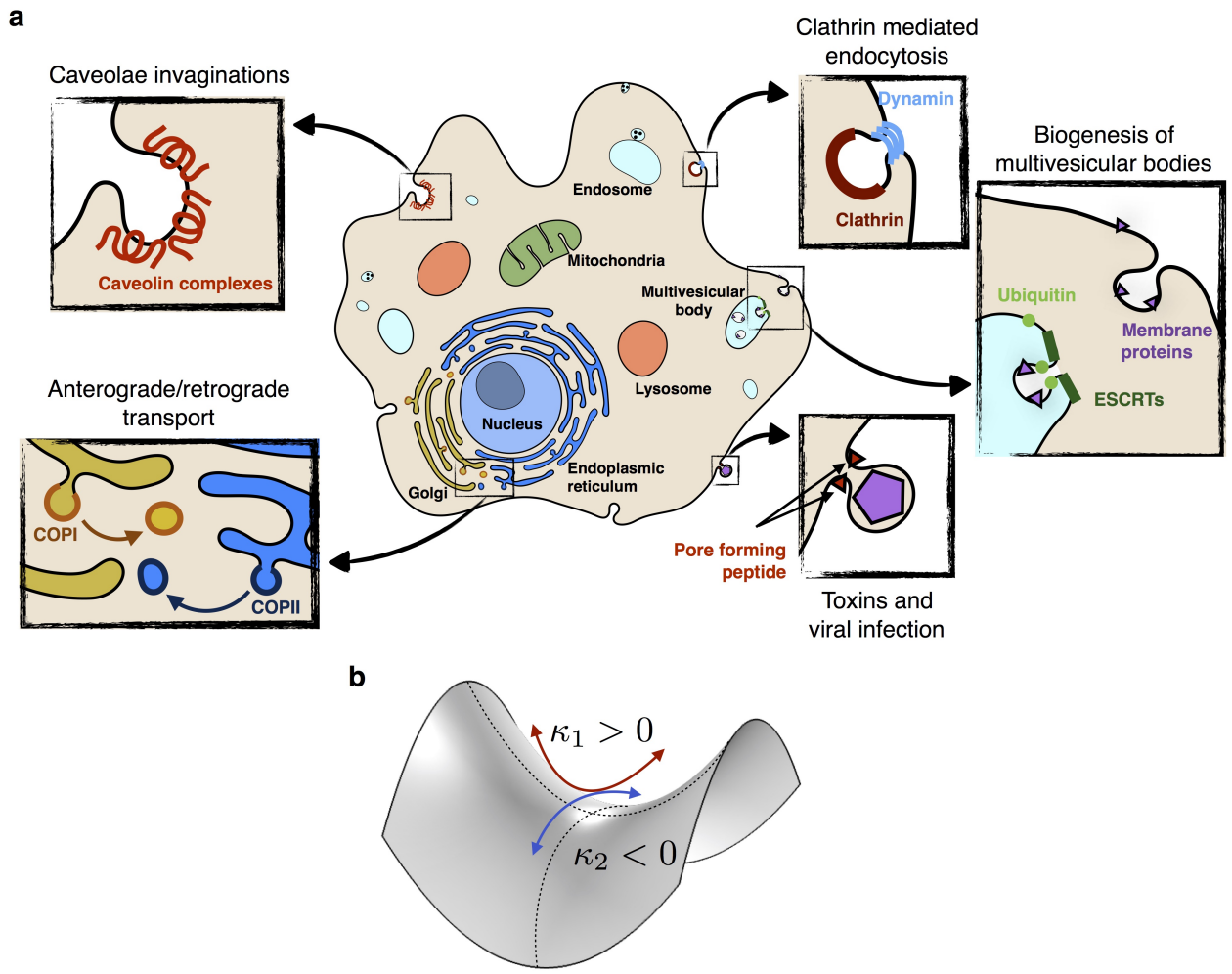

Figure 1. Necks are ubiquitous in cellular membranes. (a) The formation of necks by cellular membranes is critical for fission and fusion. A large variety of biological processes and molecular mechanisms are involved in the formation of necks; however, a common feature of these structures is that they share a catenoid-like shape. Here, we explore the relationship between catenoids and protein-induced spontaneous curvature and discuss the implications for the formation of necks. (b) The local geometry of a surface can be described by its two principal curvatures κ_1 and κ_2. When these are of opposite signs, the Gaussian curvature $K = \kappa_1 \kappa_2$ is negative, resulting in saddle shapes. Additionally, when the principal curvatures have equal and opposite values, the mean curvature $H = \kappa_1 + \kappa_2$ is zero. Surfaces with zero mean curvature are known as minimal surfaces and include catenoids.

The energy density of the membrane including the spontaneous curvature is given by

$$w(H,K,C) = k\left[H - C(\theta^1,\theta^2)\right]^2 + k_G K\,, \tag{1}$$

where H is the mean curvature, K is the Gaussian curvature, k is the bending modulus, k_G is the Gaussian modulus, and $C(\theta^1,\theta^2)$ is the spontaneous curvature field that can explicitly depend on the surface coordinates (θ^1,θ^2).

Minimizing the energy of the membrane allows us to obtain the equilibrium shape equation[26,27,33], the solution to which gives the relationship between the membrane geometry and constraints. For a membrane energy described by Eq. 1 with spatially varying spontaneous curvature and no externally applied force, the shape equation – corresponding to the normal variation of the energy – can be written as[27,31,34]

$$k\Delta(H-C) + 2k(H-C)(2H^2-K) - 2kH(H-C)^2 = p + 2\lambda H, \tag{2}$$

where p and λ are Lagrange multipliers that are interpreted as the pressure difference across the membrane, and the surface tension respectively. In this work, the differential operators $\Delta(\cdot)$ and $\nabla(\cdot)$ refer to the *surface* Laplacian and gradient respectively. The corresponding tangential equilibrium equation restricts the variations of the surface tension[27,34] so that

$$\nabla\lambda = 2k(H-C)\nabla C. \tag{3}$$

This equation is the membrane incompressibility condition.

Application to catenoids. Catenoids belong the to the mathematical family of minimal surfaces, which locally minimize their surface energy everywhere[29,35,36]. These have been historically studied in the context of soap films and the formation of membrane tethers[28,29,37,38] and more recently in the context of shapes adopted by organelle membranes[39–41].

We consider a catenoid of height H_0 and neck radius r_n such as the one depicted in Fig. 2(a). In axisymmetric coordinates, this surface can be parametrized by

$$r = r_n \cosh(z/r_n) \quad \text{with } z \in [-H_0/2; H_0/2]\ . \tag{4}$$

We seek the distribution of spontaneous curvature along the arclength $s = r_n \sinh(z/r_n)$ in the axial direction. We choose the total arclength $L = 2r_n \sinh(H_0/r_n)$, as the characteristic length of the catenoid.

The shape equation (Eq. 2) involves two geometrical invariants of the surface: the mean and the Gaussian curvature. The mean curvature is zero everywhere on a catenoid; however the Gaussian curvature of a catenoid depends on z and the neck radius as

$$K = -\left[\frac{1}{r_n \cosh^2(z/r_n)}\right]^2 = -\left[\frac{1}{r_n(1+(s/r_n)^2)}\right]^2. \tag{5}$$

The Gaussian curvature of the catenoid is negative everywhere and is minimum when $z = 0$ or $s = 0$ (Figs. 2(b) and 3(b)). As the neck radius decreases, the Gaussian curvature at the neck decreases towards minus infinity, while it tends to zero away from the neck.

For a minimal surface, the shape equation Eq. 2 and the incompressibility condition Eq. 3 reduce to

$$\Delta C - 2KC = 0\ , \tag{6}$$

$$\nabla\lambda = -2kC\nabla C = -k\nabla(C^2)\ . \tag{7}$$

This system is subject to boundary conditions. These can either be the bending moments and tractions specified along the boundary[42,43] or the spontaneous curvature specified at the boundary. Since our interest is in protein-mediated effects, we specify the spontaneous curvature at the boundaries with the following Dirichlet boundary conditions:

$$C = \begin{cases} C_0 & \text{at the lower boundary} \\ C_1 & \text{at the upper boundary} \end{cases}, \tag{8}$$

where C_0 and C_1 are prescribed. These conditions represent, for instance, two reservoirs of spontaneous curvature-inducing proteins connected to each side of the catenoid.

Non-dimensionalization and numerical implementation. We non-dimensionalize Eqs. 6, 7, and 8, using the total arclength of the symmetric catenoid L, and the reference value of spontaneous curvature at one of the boundaries C_0. Accordingly, the geometric variables are scaled as $\bar{\theta}^\alpha = \theta^\alpha/L$, and $\bar{K} = KL^2$, while the spontaneous curvature is scaled as $\bar{C} = C/C_0$. Eqs 6 and 7 therefore become

$$\Delta\bar{C} - 2\bar{K}\bar{C} = 0, \tag{9}$$

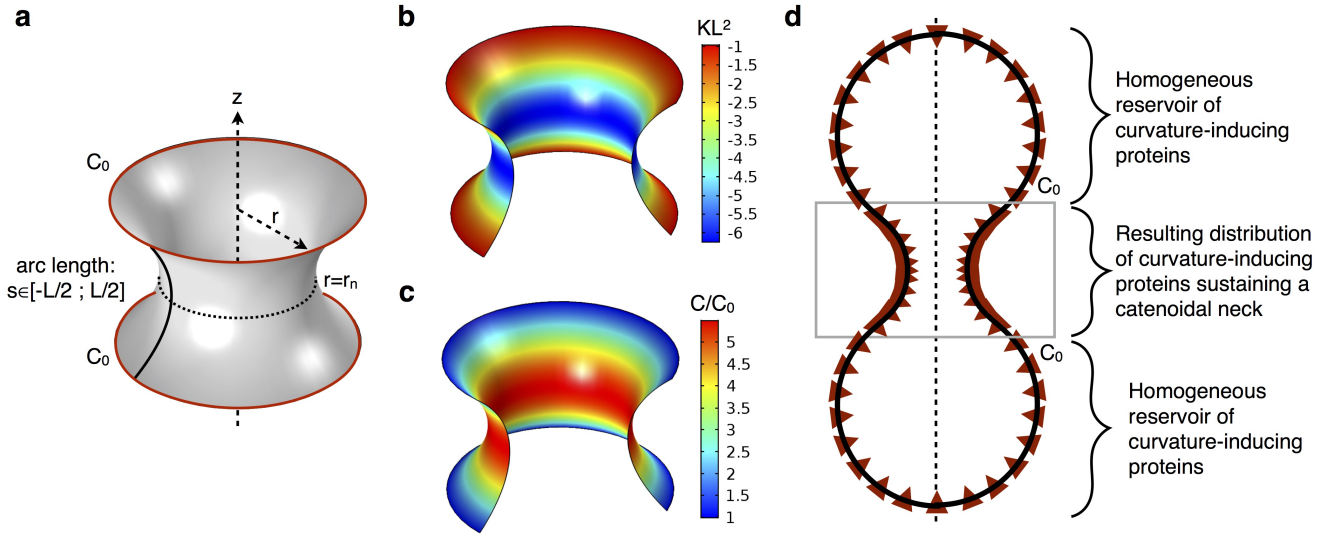

Figure 2. Given a neck radius r_n, a catenoid-shaped neck connected to two identical reservoirs of curvature-inducing proteins shows a variation of spontaneous curvature along the arclength. (a) Geometry and boundary conditions of the catenoid. The arclength s varies from $-L/2$ to $L/2$ and the boundary conditions are $C = C_0$. (b) Variation of dimensionless Gaussian curvature K/L^2 on a catenoid of neck radius $r_n = 0.4L$. (c) Corresponding distribution of dimensionless spontaneous curvature. (d) Schematic of a possible spontaneous curvature inducing protein distributed along a catenoid connecting two vesicles. The two spherical parts are protein reservoirs imposing spontaneous curvature at the boundaries of the catenoid, and resulting in a distribution of curvature-inducing proteins along the neck.

and

$$\frac{\lambda - \lambda_0}{kC_0^2} = -\bar{C}^2 \,. \tag{10}$$

with the non-dimensional boundary condition

$$\bar{C} = \begin{cases} 1 & \text{at the lower boundary} \\ C_1/C_0 & \text{at the upper boundary} \end{cases} \,. \tag{11}$$

Eqs. 9-11 completely describe the system. Since Eq. 11 is decoupled from Eq. 9, the tension across the membrane can be calculated *post facto* from the spontaneous curvature distribution. Therefore, we will not discuss the tension in the catenoid going forward.

The total energy of the membrane is defined by the integral of the energy density over the catenoid surface

$$W = \int \left(kC^2 + k_G K\right) dA \,. \tag{12}$$

In non-dimensional form, the total energy is written

$$\frac{W}{kC_0^2 L^2} = \int \left(\bar{C}^2 + \frac{k_G}{k}\frac{1}{C_0^2 L^2}\bar{K}\right) d\bar{A} \,. \tag{13}$$

Dividing by the non-dimensionalized area of the catenoid $\bar{A} = A/L^2$, the non-dimensional energy per area is $W/(kC_0^2 A)$. We use the value $k_G/k = -0.9$ for the ratio of the Gaussian to bending modulus[44] .

Eq. 9 is a variable coefficient Helmotz equation that, to our knowledge, lacks an analytic solution. Therefore, we solve the system composed of Eqs. 9 and 11 with the finite element solver Comsol Multiphysics 5.2a, and the 'Surface reaction' module that has a built-in surface Laplacian. Parametric studies are conducted by exploiting the COMSOL model with the 'COMSOL with Matlab' module.

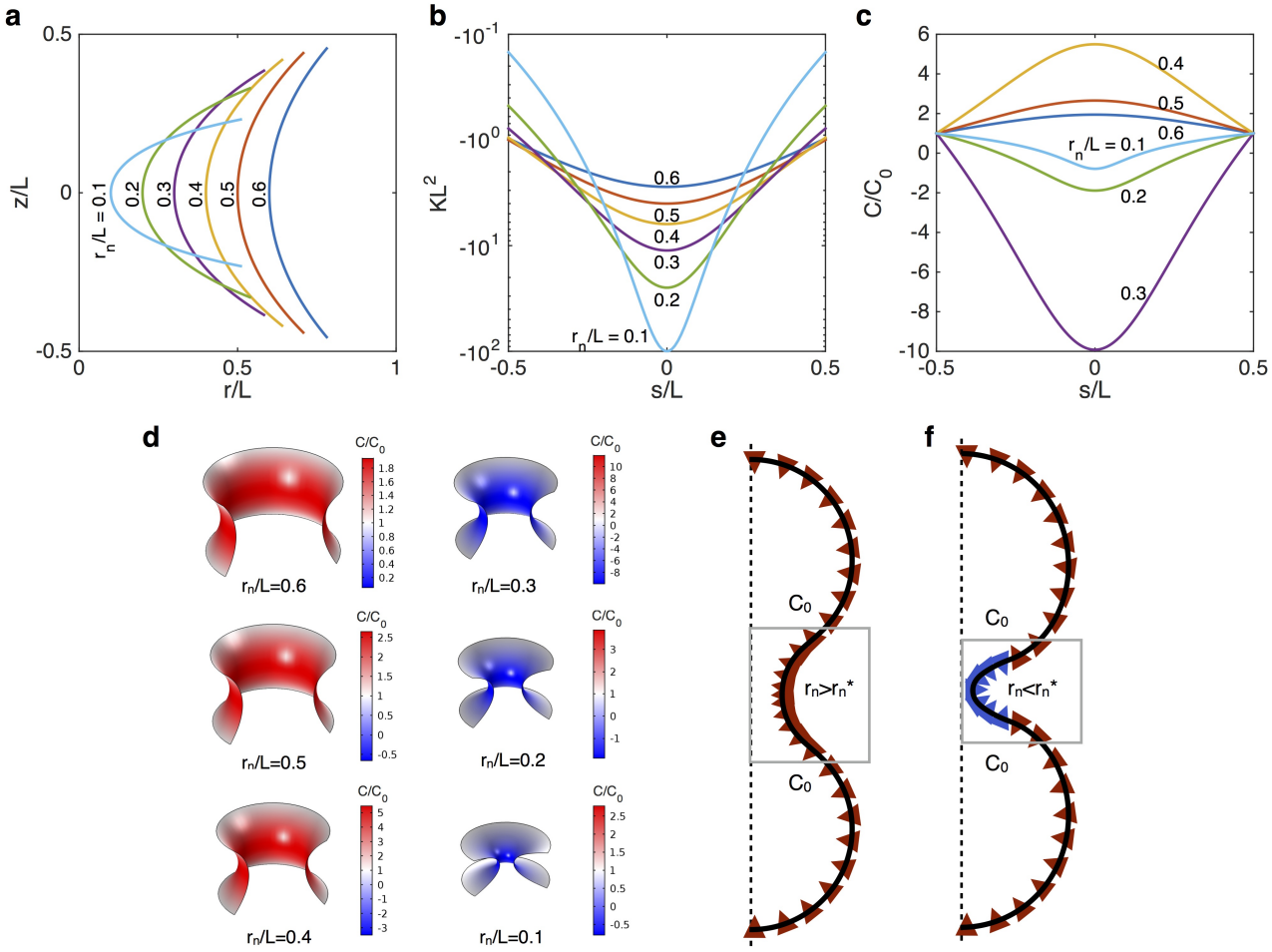

Figure 3. Constraining the neck of a catenoid induces a switch in the sign of spontaneous curvature at constant total arclength and boundary conditions. (a) Axisymmetric geometry of six catenoids of various neck radii r_n and same total arclength L. (b) Dimensionless Gaussian curvature along the arclength s for various neck radii. (c) Resulting spontaneous curvature along the arclength for $C = C_0$ at both boundaries. (d) Corresponding distribution of spontaneous curvature on the catenoid. (e, f) Schematics of a distribution of curvature inducing proteins on a catenoid connecting two vesicles. (e) For a catenoid-shaped neck of radius larger than the critical radius $r_n > r_n^*$, only proteins inducing a spontaneous curvature of the same sign as C_0 are required to sustain the catenoid. (f) When the neck radius is below the critical neck radius $r_n < r_n^*$, proteins with spontaneous curvature of opposite sign as C_0 are necessary to sustain the catenoid-shaped neck.

Results

The Gaussian curvature of the catenoid governs the distribution of spontaneous curvature. We begin our analysis with the catenoid shown in Fig. 2(a) with a total arclength L and neck radius $r_n = 0.4L$. The geometry of a catenoid determines its Gaussian curvature along its arclength through Eq. 5. The Gaussian curvature of the catenoid considered here is displayed in Fig. 2(b). As expected K is negative everywhere, with a maximum amplitude at the neck. How does the Gaussian curvature affect the distribution of protein-induced spontaneous curvature? We answer this question by solving the boundary value problem composed of Eq. 9 with $C = C_0$ at both boundaries (see Fig. 2(a)). The resulting field of spontaneous curvature is shown in Fig. 2(c). For this configuration, the spontaneous curvature is positive everywhere with a maximum at the neck, following the intensity of Gaussian curvature.

In order to interpret this spatially varying spontaneous curvature, one can think of the inclusion of a single type of conic protein into the lipid bilayer. In this case, a catenoid with fixed spontaneous curvature at the boundaries can

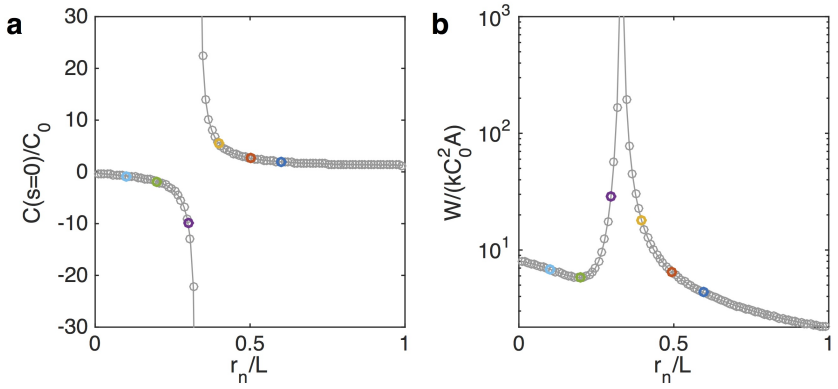

Figure 4. The switch of spontaneous curvature at the neck is accompanied by an energy barrier of the catenoid. (a) Normalized membrane spontaneous curvature at the neck as a function of the neck radius. (b) Energy per area of a catenoid as a function of the dimensionless neck radius. (Color symbols correspond to neck radii configurations shown in Fig. 3(a-c). Solid line is a visual guide.).

be schematically represented as in Fig. 2(d), where two reservoirs of the curvature-inducing protein are connected to the boundaries. A variation of spontaneous curvature along the catenoid corresponds to a variation of protein surface density along the neck. The value of C as a function of protein density depends on the protein and on the curvature inducing mechanism[18].

The energy required to maintain a catenoid-shaped membrane through spontaneous curvature presents a barrier at a critical neck radius. The radius of the neck is an important geometric parameter of catenoids, and is of particular interest to pre-fusion events in trafficking[1–4]. We next investigate how the neck radius influences the distribution of spontaneous curvature along a catenoid. We vary the neck radius between $r_n = 0.1L$ and $r_n = 0.6L$ as shown in Fig. 3(a). The resulting Gaussian curvatures along the arclength, presented in Fig. 3(b), show an increase of the curvature intensity at the neck as the neck decreases. Away from the neck however, a smaller neck radius produces a lower Gaussian curvature.

We solve the boundary problem for the spontaneous curvature, resulting in the distribution of C depicted in Fig. 3(c). The boundary conditions are the same as the one shown in Fig. 2(a), with $C = C_0$ at both boundaries, corresponding to a neck connected to two equal reservoirs of curvature inducing proteins. Although the maximum of spontaneous curvature intensity is always at the neck, its value is a non-monotonic function of the neck radius and Gaussian curvature. For large neck radii, decreasing r_n increases the maximum of C, until a critical neck radius r_n^* below which C at the neck switches signs. After this switch, further decreasing the neck radius lowers the intensity of spontaneous curvature. Fig. 3(d) shows the distribution of spontaneous curvature on the catenoids for the corresponding radii.

This non-intuitive switch-like behavior is surprising because neither the neck radius nor the resulting Gaussian curvature show a discontinuity. Furthermore, the boundary conditions for the spontaneous curvature are constant $C = C_0$. An intuitive understanding of this behavior can be obtained by considering a simplified case where the Gaussian curvature K is constant along the arclength, reducing the shape equation for minimal surfaces to a one-dimensional simple harmonic oscillator. As shown in the Appendix, in this simplified case, reducing the neck radius is equivalent to decrease the period of the oscillator, which, when subject to fixed non-zero boundary conditions, leads to a series of diverging values for $r_n^*/L \sim \sqrt{2}/[\pi(1+2n)]$, with $n \in \mathbb{Z}$. For $n = 0$ we obtain $r_n^*/L \simeq 0.45$, close to the value observed in Fig. 4 for the catenoid. Interestingly, the value of neck radius at which the switch occurs does not depends on the value of the boundary condition, but only on the total arclength. Note that other critical values are expected for $n \neq 0$, and although these are observed for a constant K (see Appendix), in the case of the catenoid, K tends to zero away from the neck, suppressing the other possible switches.

The switch in sign of the spontaneous curvature as a function of neck radius can be interpreted as a requirement

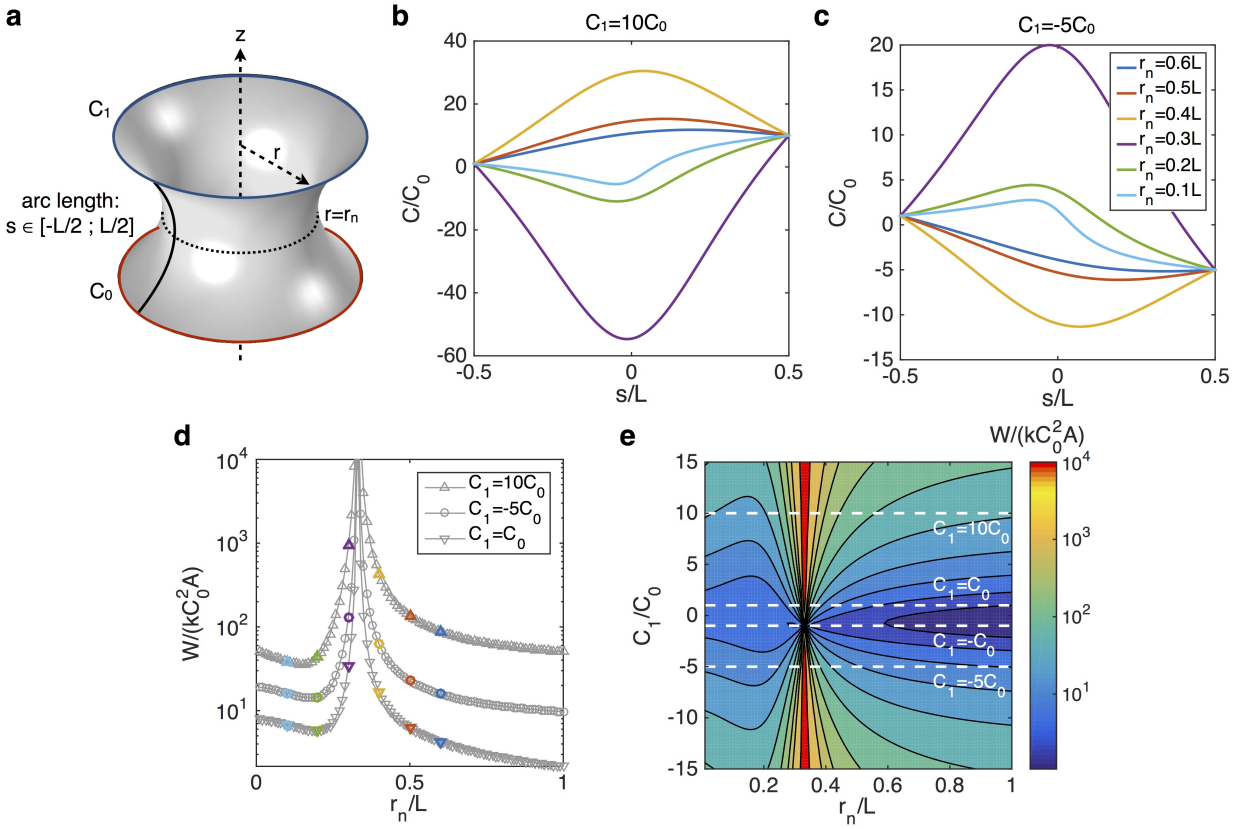

Figure 5. A spontaneous curvature differential between the two boundaries determines the width of the associated energy barrier but does not influence the position of the switch in spontaneous curvature. (a) Schematic of a catenoid with unequal boundary conditions. (b) Distribution of spontaneous curvature along the arclength for $C_1/C_0 = 10$ for various neck radii. (c) Distribution of spontaneous curvature along the arclength for $C_1/C_0 = -5$. (d) Comparison of the energy per area of the catenoid for various boundary conditions. The larger the spontaneous curvature differential at the boundary, the larger the energy barrier corresponding to the sign switch. (e) Contour plot of the energy per area for C_1/C_0 varying between -15 and 15 as a function of the neck radius. The energy barrier (warm colors) is located around a constant critical neck radius of about $r_n^* = 0.33L$.

that another set of proteins with spontaneous curvature opposite to the one in the reservoir will be needed to minimize the energy of catenoids with smaller necks. This idea is shown in Figs. 3(e) and (f), where possible distributions of curvature-inducing proteins are depicted for necks larger and smaller than the critical radius.

To further identify the relationship between the switch in spontaneous curvature and the geometry, we plot in Fig. 4(a) the spontaneous curvature at the neck as a function of r_n. These results confirm the switch-like behavior described above and in the vicinity of a critical neck radius $r_n^* \simeq 0.33L$, the spontaneous curvature at the neck diverges, with positive values above r_n^*, and negative values below. In the two limits of large and small neck radii, the spontaneous curvature tends to C_0 everywhere. This is consistent with the two limit shapes of a catenoid: a tube and two inverted cones, both of which have a zero Gaussian curvature, and therefore no spatial variation of spontaneous curvature.

As show in Fig. 4(b), the energy to stabilize a catenoid-shaped neck through spontaneous curvature also shows an energy barrier at the critical neck radius r_n^* corresponding to the switch in C. Away from this energy barrier, the radius of the neck can be reduced by small increases in the elastic energy of the system. The passage from one side to the other of the energy barrier will require additional mechanisms such as relaxation of the boundary conditions, external forces (e.g. actin pulling in clathrin mediated endocytosis[45]), or a transient geometrical deviation from a

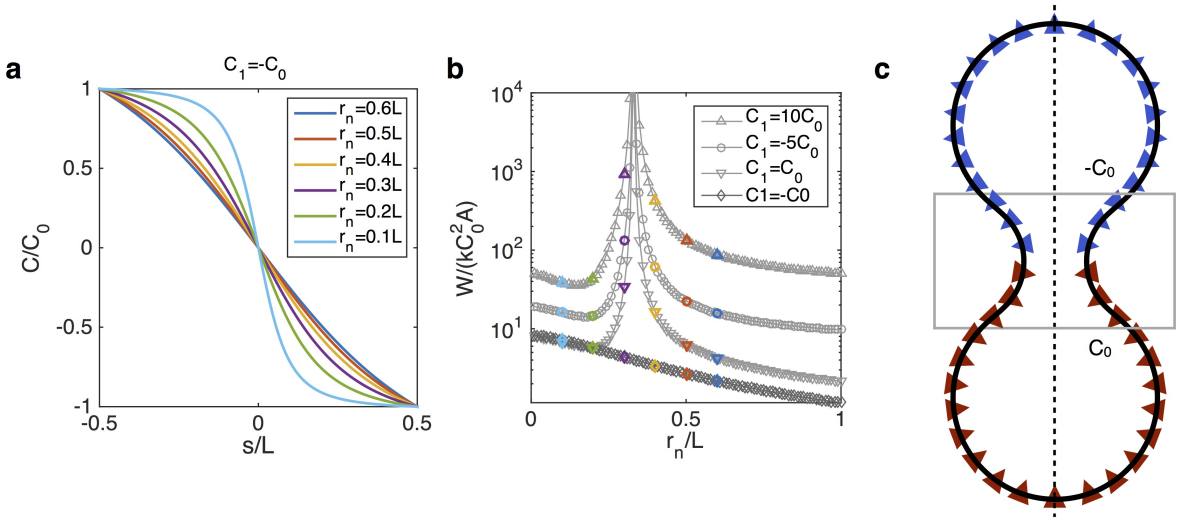

Figure 6. For boundary conditions where the spontaneous curvature have opposite values ($C_1 = -C_0$), the switch in the sign associated with the neck radius is nullified, and the spontaneous curvature at the neck is zero. (a) Spontaneous curvature along the arclength of a catenoid with $C_1 = -C_0$ for various neck radii. (b) Energy per area of the catenoid as function of the neck radius; no energy barrier is observed for $C_1 = -C_0$. (c) Schematic of a catenoid connecting two vesicles with curvature inducing proteins of opposite signs at the two spherical reservoirs. The smooth transition from C_0 to $-C_0$ requires a zero spontaneous curvature at the neck.

symmetric catenoid. In the following, we investigate how the energy barrier in the catenoid-shaped neck can be modulated by spontaneous curvature and geometry.

The differential in spontaneous curvature between the boundaries modulates the intensity of the energy barrier. How do the boundary conditions influence the distribution of spontaneous curvature in the neck? We consider the catenoid represented in Fig. 5(a), where the spontaneous curvature at the upper boundary is $C_1 \neq C_0$. This situation is likely to occur in a cellular context where the heterogeneous membrane composition may produce a differential in spontaneous curvature across the neck. We find that the switch-like behavior in spontaneous curvature persists independently of the ratio C_1/C_0. As shown in Figs. 5(b) and (c), the distribution of C is tilted to accommodate the boundary conditions, and the sign of the extremum is determined by the boundary condition with the largest absolute value. However the critical radius at which the switch occurs remain the same. This is better seen in Fig. 5(d), where the critical radius associated with the energy barrier is independent of C_1. This observation is consistent with the expression for the critical neck obtained with the simple oscillator analogy that is independent of the boundary conditions (see Eq. A6).

To fully explore the influence of the spontaneous curvature differential at the boundaries, we computed the energy of the catenoid for a wide range of C_1/C_0 as a function of r_n (Fig. 5(e)). The results confirm the behavior described above, except for $C_1 = -C_0$ where a singularity seems to occur. The spontaneous curvature profile in this case, where the boundary of the catenoid have opposite curvatures, is shown in Fig. 6(a). Here the switch in spontaneous curvature is suppressed, and $C = 0$ at the neck independently of the neck radius. Correspondingly, the energy barrier vanishes as seen in Fig. 6(b). Once again, this scenario can be interpreted as a neck connecting two reservoirs of proteins with the same magnitude of curvature but in opposite directions (see Fig. 6(c)). The boundary conditions produce smooth transition from C_1 to C_0 along the catenoid, transiting by $C = 0$ at the neck. This result is evident from the simple oscillator analogy, where the spontaneous curvature at the neck is proportional to $C_0 + C_1$ (see Eq. A4), and is therefore invariably zero for $C_1 = -C_0$.

Interestingly, the energy per unit area away from the barrier suggests that for a large spontaneous differential at the boundaries, a small neck radius is energetically favorable compared to a large neck radius. This result contrasts with the case $C_1 = C_0$, where large neck radii are favorable. The variation of spontaneous curvature differential

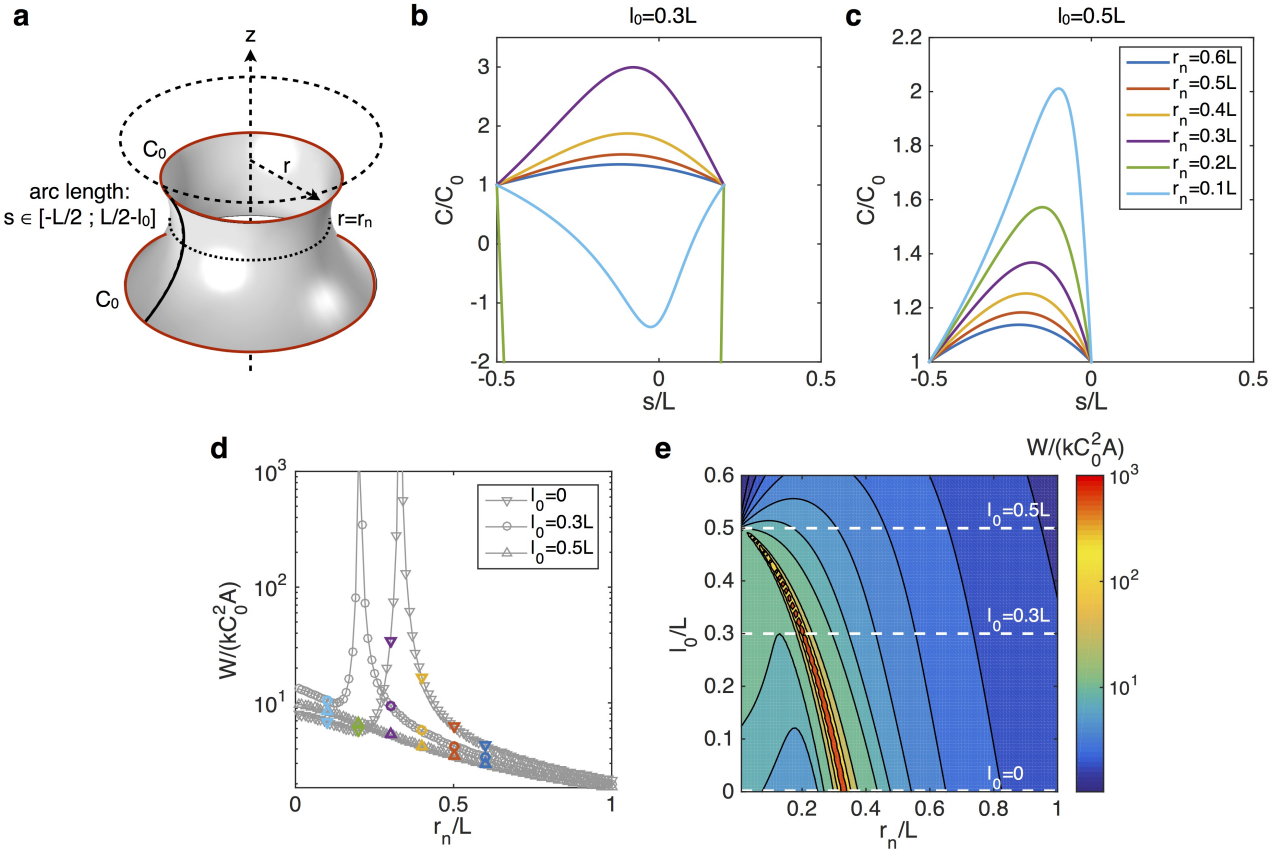

Figure 7. Asymmetry along the catenoid arclength determines the value of neck radius at which the spontaneous curvature sign switches. (a) Schematic of the geometry of the catenoid with a truncated arclength $L - l_0$. (b, c) Distribution of spontaneous curvature along the arclength for l_0/L =0.3 (b) and l_0/L =0.5 (c), for various neck radii. (d) Comparison of the energy per area of the catenoid for various degrees of asymmetry. The more truncated, the smaller value of the critical neck radius. For a half catenoid ($l_0/L = 0.5$), the energy barrier and the sign switch disappear. (e) Contour plot of the energy per area for l_0/L varying between 0.1 and 0.6 as a function of the neck radius.

across the neck may be a mechanism cells utilize to modulate the energy to form a neck. In particular, by accessing the large heterogeneity available due to membrane lipid composition and proteins, cells can disrupt the energy barrier associated with the transition from a large to a small neck radius, and *vice versa*.

The catenoid geometrical asymmetry modulates the location of the energy barrier. Thus far, we have only considered catenoids that are geometrically symmetric, that is, both sides of the neck have equal arc length. Yet, asymmetric catenoids are more common in the cellular environment. For instance, the neck connecting a tube to a larger membrane reservoir is a catenoid partially truncated[22,46]. We therefore ask how does geometric asymmetry influence the distribution of spontaneous curvature and energy associated witht the switch?

We conduct simulations on truncated catenoids of arc length $L - l_0$ as shown in Fig. 7(a), with both boundaries subject to the same spontaneous curvature C_0. The profile of spontaneous curvature along the arclength are shown for different degrees of geometrical asymmetry in Figs. 7(b) and (c). We find that reducing asymmetry in the catenoid modifies the critical neck radius at which the switch in spontaneous curvature occurs. As seen from Figs. 7(d) and (e), where the energy of the catenoid is plotted as a function of the neck radius, the larger the degree of asymmetry l_0, the smaller the critical neck radius at which the energy barrier occurs. Once half or more of the catenoid is cut off, corresponding to $l_0 \geq L/2$, the energy barrier completely vanishes, allowing the neck radius to transition from

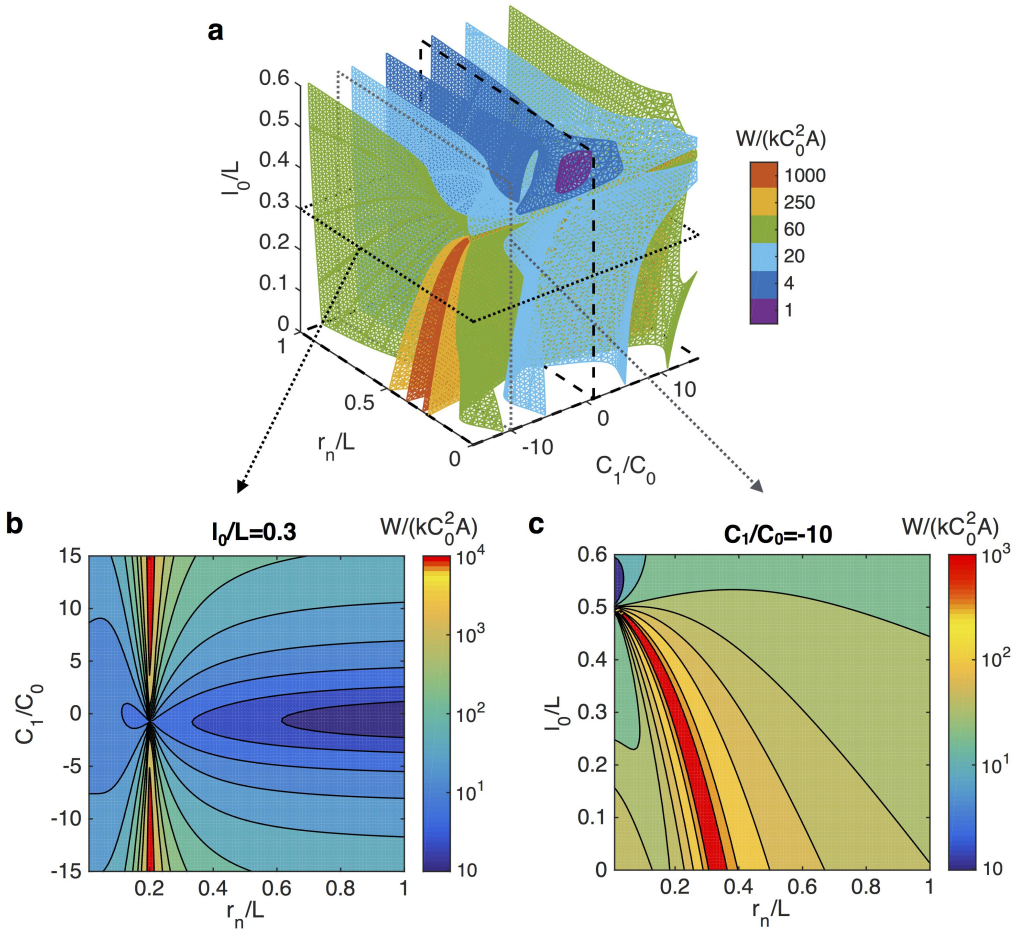

Figure 8. Total energy per unit area of catenoids in the parameters space defined by dimensionless neck radius (r_n/L), spontaneous curvature asymmetry (C_1/C_0), and geometrical asymmetry (l_0/L). (a) Isosurfaces of the energy. The two dashed planes correspond to the energy landscapes shown in Fig. 5(e) and 7(e). The dotted planes correspond to energy landscapes for $l_0/L = 0.3$ shown in (b), and $C_1/C_0 = -10$ shown in (c).

large to small values through spontaneous curvature mechanisms only.

For completeness, we fully explore all the combinations of spontaneous curvature differential and geometric asymmetry of the catenoid by computing the corresponding energy space. As shown in Fig. 8(a), the results confirm the behaviors described above, where the differential in C across the neck mainly influences the width and intensity of the energy barrier, while the geometrical asymmetry determines the critical neck radius corresponding to the energy barrier and the switch. This is further shown in the two energy isovalue planes presented in Figs. 8(b) and (c) which have overall similar behaviors as those plotted in Figs. 5(e) and 7(e) respectively.

Discussion

Necks are ubiquitous in membrane biology, appearing as a necessary step in vesiculation processes and connecting tubules to membranes reservoirs. These structures can be studied and understood as catenoids[21,24], which are minimal surfaces with zero mean curvature and negative Gaussian curvature everywhere. The formation of necks has been associated with line tension[47], the change in Gaussian modulus[12] and other forces, but the interaction between spontaneous curvature and Gaussian curvature has not been explored until now.

In this study, we explore the intricate relationship between Gaussian curvature, spontaneous curvature, and neck geometry. We asked, given a neck geometry, what spontaneous curvature field would satisfy the minimum energy

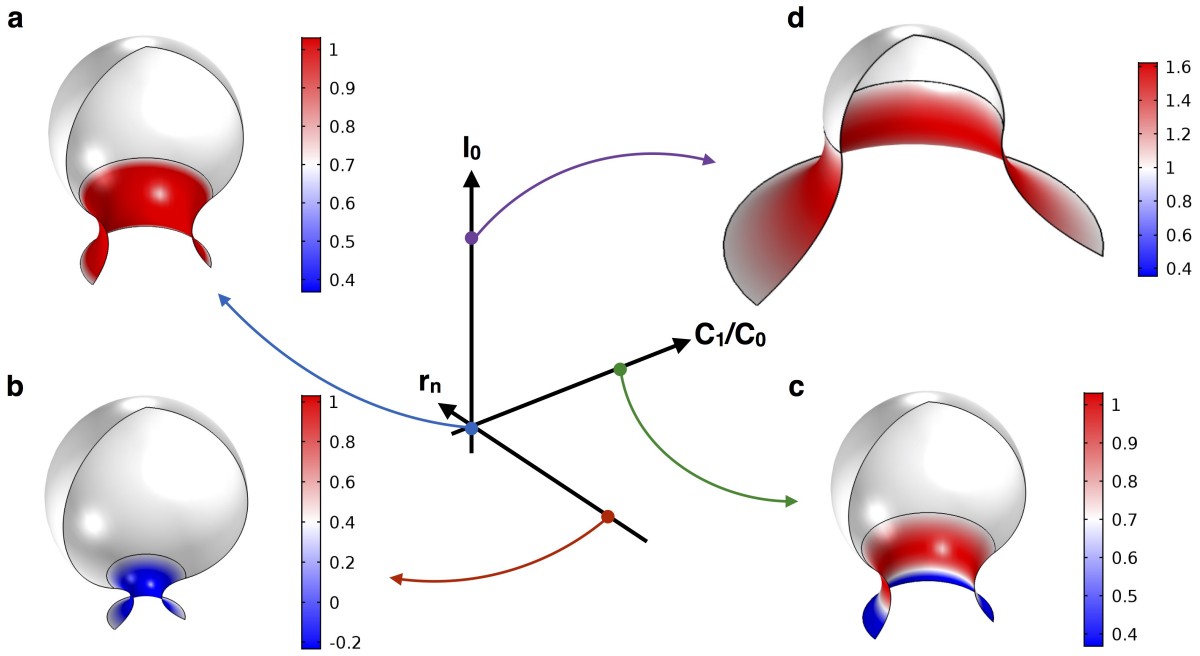

Figure 9. Three features control the distribution of a spontaneous curvature along a catenoid-shaped neck, the neck radius, the boundary conditions, and the asymmetry of the catenoid. These can be utilized to form or maintain buds connected to a reservoir of curvature inducing proteins through a catenoid.

requirement for a bilayer. We found a rather non-intuitive answer: the spontaneous curvature field depends on the Gaussian curvature and its intensity follows a switch-like behavior depending on the neck radius of the catenoid. The catenoid-shaped neck has an energy barrier at a critical neck radius corresponding to the switch in the sign of the spontaneous curvature. We further identified two mechanisms allowing the modulation of this energy barrier – (i) amplifying the spontaneous curvature differential at the boundaries increases the intensity and width of the energy barrier (Fig. 5) and (ii) the geometrical asymmetry of the catenoid determines the critical neck radius at which the energy barrier is located (Fig. 7). Moreover we found that the switching behavior is lost in specific cases: when the spontaneous curvature at the boundaries have opposite value (Fig. 6), and when half or more of the catenoid is truncated (Fig. 7).

Spontaneous curvature of lipid bilayers can be produced by a variety of relatively well understood mechanisms[16,19,20]. In particular, the insertion of amphiphatic α-helix into lipid bilayers is known to induce curvature and is involved in several neck formation processes. Amphiphatic α-helixes is a conserved protein structure that can be found in Arf1 (involved in COP vesicle intracellular trafficking[48]), Epsin (involved in actin and clathrin mediated endocytosis[49]), and M2 proteins from influenza virus (involved in viral budding[5,8,50]). All of these proteins have been shown to participate in membrane fission, which corresponds to the limiting shape of neck constriction[4,8,48]. A similar mechanism is utilized by antimicrobial peptides (AMPs) to form buds and destabilize lipid membrane by inducing negative Gaussian curvature[6,7,51].

One of the main findings of this study is the existence of an energy barrier for catenoid-shaped necks at a certain neck radius. This energy barrier is accompanied with a switch in the sign of spontaneous curvature along the catenoid. This behavior can be related to several biological mechanisms relevant to neck formation and membrane fission. Several studies have shown that lipids with negative spontaneous curvature are important during the fission process[7,52–54]. We found that a change in the sign of the spontaneous curvature is important to overcome the energy barrier associated with reducing neck size. Therefore, it is possible that by harnessing the heterogeneity of lipid species[55], and chemical reactions that can lead to the formation of lipids with negative spontaneous curvature,

pre-fission structures overcome the energy barrier associated with necks.

For instance, viral budding in influenza occurs in two main steps. First a neck is formed by a combination of scaffolding and lipid phase separation originating from the viral envelope. This step can only produce a neck of about 25 nm diameter, necessitating the action of another mechanism to further constrain the neck. During the second step, M2 amphiphatic α-helix insertion induces negative Gaussian curvature enabling the neck radius to reach values below 5 nm[8,50], at which point spontaneous membrane scission can occur[2,47]. It should be noted that no necking is possible with M2 amphiphatic α-helix only[8]. The requirement for two distinct mechanisms in two regions of neck radii could be related to the energy barrier that we found as the neck radius of the catenoid decreases. Other evidence of switch-like behaviors are found in endocytosis where multiple studies have reported the existence of a snap-through instability[30,31,56,57]. Furthermore, soap films, with no bending rigidity, also exhibit a structural instability when held as catenoids[37,58]. Taken together, these findings suggest that perhaps, cellular membranes may utilize a fundamental geometric feature of catenoids to shape their membranes.

While our model assumes an idealized catenoid shape for membrane necks, it is possible that necks may not remain as exact catenoids and the dynamics of the neck formation process, including biochemical reactions, heterogeneity in membrane composition and moduli, forces exerted by proteins and cytoskeleton molecules, and in-plane diffusion of lipids and proteins play an important role during fission and fusion. Despite these shortcomings, we have identified some fundamental features of the interaction between Gaussian curvature and spontaneous curvature in catenoids. We summarize our findings as a phase space where the spontaneous curvature, neck radius, and the geometric asymmetry of the catenoid can be altered to obtain buds and necks of different radii (Fig. 9). These variables might serve as design parameters for artificial membrane constructs and a stepping stone for further investigation of how membrane geometry and proteins interact.

Appendix: Simple Oscillator Analogy

In order to study the behavior of Eq. 6 in simplified conditions, let us consider the case where K is a constant. In one-dimension, Eq. 6 can now be written as

$$\frac{d^2C}{ds^2} = -\omega^2 C\,, \tag{A1}$$

where $\omega^2 = -2K$ is a positive constant, and $s \in [-L/2; L/2]$. This is the equation of a simple harmonic oscillator of period $T = 2\pi/\omega = \pi\sqrt{-2/K}$, which has for general solution

$$C(s) = A\cos(\omega s) + B\sin(\omega s)\,, \tag{A2}$$

A and B being constants determined by the boundary conditions. With boundary conditions $C(-L/2) = C_0$ and $C(L/2) = C_1$ the solution is

$$C(s) = \frac{C_0 + C_1}{2\cos(\omega L/2)}\cos(\omega s) - \frac{C_0 - C_1}{2\sin(\omega L/2)}\sin(\omega s)\,. \tag{A3}$$

From Eq. A3 we have that the value of C at the neck ($s = 0$) is

$$C(0) = \frac{C_0 + C_1}{2\cos(\omega L/2)}\,, \tag{A4}$$

which diverges for $\omega^* = (\pi + 2n\pi)/L$, where $n \in \mathbb{N}$. Or in terms of the oscillator period, the solution diverges for

$$T^* = \frac{2L}{1+2n}\,. \tag{A5}$$

Eq. A3 is plotted in Fig. 10 for various periods T. The value of C within the interval $[-L/2; L/2]$ is positive for $T > T^*(n = 1)$, and negative below. To decrease the oscillator period is conceptually equivalent to increase the

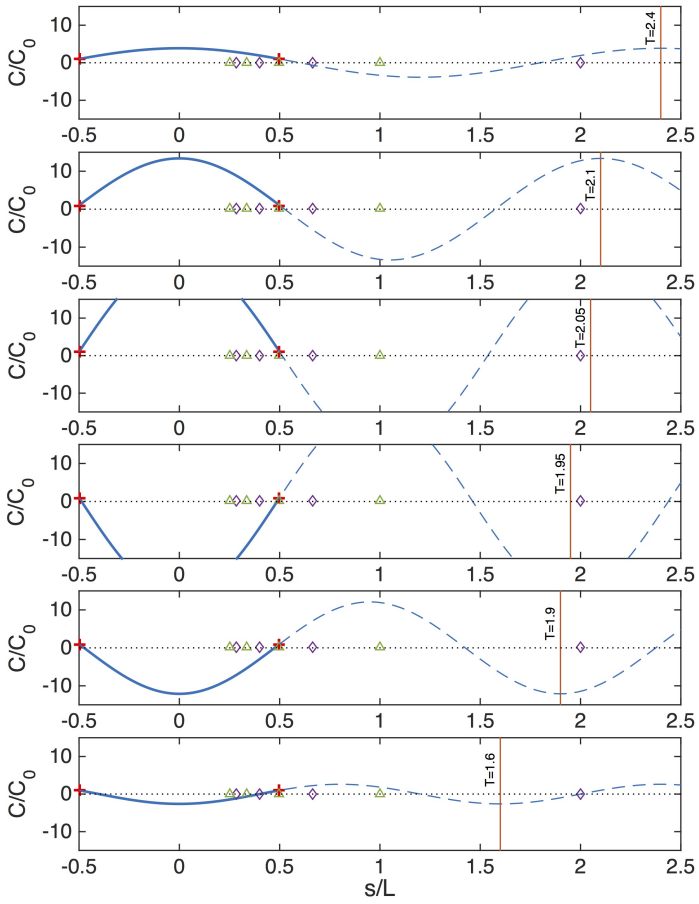

Figure 10. The switch-like behavior in spontaneous curvature observed for catenoids can be conceptually understood with a simple oscillator. The solution of a simple harmonic oscillator (Eq. A3) with $C_1 = C_0$ depends on the oscillator period $T = -\pi/K$. Decreasing values of the oscillator period correspond to increasing values of K, and therefore decreasing values of the neck radius. C diverges for $T^*/L = 2/(1+2n)$ (marked by purple diamonds), and changes mode for $T^*/L = 1/(1+n)$ (indicated by green triangles).

absolute value of K, or to decrease the neck radius of the catenoid. For a catenoid, the Gaussian curvature at the neck is $K(s=0) = -1/r_n^2$. Taking $\omega^2 = 2/r_n^2$, the positive value of the neck radius for which the spontaneous curvature diverges is

$$r_n^* = \frac{\sqrt{2}L}{\pi(1+2n)} \,. \tag{A6}$$

For $n = 0$, we have $r_n^*/L \simeq 0.45$. From Eq. A6, it is clear that the value of the critical neck radius is independent of the boundary conditions.

References

1. Hurley, J. H. & Hanson, P. I. Membrane budding and scission by the ESCRT machinery: It's all in the neck. *Nat. Rev. Mol. Cell Biol.* **11**, 556–566 (2010). DOI 10.1038/nrm2937.

2. Campelo, F. & Malhotra, V. Membrane Fission: The Biogenesis of Transport Carriers. *Annu. Rev. Biochem.* **81**, 407–427 (2012). DOI 10.1146/annurev-biochem-051710-094912.

3. Kukulski, W., Schorb, M., Kaksonen, M. & Briggs, J. A. G. Plasma Membrane Reshaping during Endocytosis Is Revealed by Time-Resolved Electron Tomography. *Cell* **150**, 508–520 (2012). DOI 10.1016/j.cell.2012.05.046.

4. Messa, M. *et al.* Epsin deficiency impairs endocytosis by stalling the actin-dependent invagination of endocytic clathrin-coated pits. *eLife* **3**, e03311 (2014). DOI 10.7554/eLife.03311.

5. Mishra, A., Gordon, V., Yang, L., Coridan, R. & Wong, G. HIV TAT Forms Pores in Membranes by Inducing Saddle-Splay Curvature: Potential Role of Bidentate Hydrogen Bonding. *Angewandte Chemie Int. Ed.* **47**, 2986–2989 (2008). DOI 10.1002/anie.200704444.

6. Schmidt, N., Mishra, A., Lai, G. H. & Wong, G. C. Arginine-rich cell-penetrating peptides. *FEBS Lett.* **584**, 1806–1813 (2010). DOI 10.1016/j.febslet.2009.11.046.

7. Schmidt, N. W. & Wong, G. C. L. Antimicrobial peptides and induced membrane curvature: Geometry, coordination chemistry, and molecular engineering. *Curr. Opin. Solid State Mater. Sci.* **17**, 151–163 (2013). DOI 10.1016/j.cossms.2013.09.004.

8. Martyna, A. *et al.* Membrane remodeling by the M2 amphipathic helix drives influenza virus membrane scission. *Sci. Reports* **7** (2017). DOI 10.1038/srep44695.

9. Sanborn, J., Oglęcka, K., Kraut, R. S. & Parikh, A. N. Transient pearling and vesiculation of membrane tubes under osmotic gradients. *Faraday Discuss.* **161**, 167 (2013). DOI 10.1039/c2fd20116j.

10. Ho, J. C. S., Rangamani, P., Liedberg, B. & Parikh, A. N. Mixing Water, Transducing Energy, and Shaping Membranes: Autonomously Self-Regulating Giant Vesicles. *Langmuir* **32**, 2151–2163 (2016). DOI 10.1021/acs.langmuir.5b04470.

11. Baumgart, T., Hess, S. T. & Webb, W. W. Imaging coexisting fluid domains in biomembrane models coupling curvature and line tension. *Nat.* **425**, 821–824 (2003). DOI 10.1038/nature02013.

12. Baumgart, T., Das, S., Webb, W. W. & Jenkins, J. T. Membrane Elasticity in Giant Vesicles with Fluid Phase Coexistence. *Biophys. J.* **89**, 1067–1080 (2005). DOI 10.1529/biophysj.104.049692.

13. Busch, D. J. *et al.* Intrinsically disordered proteins drive membrane curvature. *Nat. Commun.* **6**, 7875 (2015). DOI 10.1038/ncomms8875.

14. Snead, W. T. *et al.* Membrane fission by protein crowding. *Proc. Natl. Acad. Sci.* **114**, E3258–E3267 (2017). DOI 10.1073/pnas.1616199114.

15. Staykova, M., Holmes, D. P., Read, C. & Stone, H. A. Mechanics of surface area regulation in cells examined with confined lipid membranes. *Proc. Natl. Acad. Sci.* **108**, 9084–9088 (2011). DOI 10.1073/pnas.1102358108.

16. Zimmerberg, J. & Kozlov, M. M. How proteins produce cellular membrane curvature. *Nat. Rev. Mol. Cell Biol.* **7**, 9–19 (2006). DOI 10.1038/nrm1784.

17. Baumgart, T., Capraro, B. R., Zhu, C. & Das, S. L. Thermodynamics and Mechanics of Membrane Curvature Generation and Sensing by Proteins and Lipids. *Annu. Rev. Phys. Chem.* **62**, 483–506 (2011). DOI 10.1146/annurev.physchem.012809.103450.

18. Lipowsky, R. Spontaneous tubulation of membranes and vesicles reveals membrane tension generated by spontaneous curvature. *Faraday Discuss.* **161**, 305–331 (2013). DOI 10.1039/C2FD20105D.

19. Jarsch, I. K., Daste, F. & Gallop, J. L. Membrane curvature in cell biology: An integration of molecular mechanisms. *The J. Cell Biol.* **214**, 375–387 (2016). DOI 10.1083/jcb.201604003.

20. Chabanon, M., Stachowiak, J. C. & Rangamani, P. Systems biology of cellular membranes: A convergence with biophysics. *WIREs Syst. Biol. Medicine* e01386 (2017). DOI 10.1002/wsbm.1386.

21. Kozlovsky, Y. & Kozlov, M. M. Membrane Fission: Model for Intermediate Structures. *Biophys. J.* **85**, 85–96 (2003). DOI 10.1016/S0006-3495(03)74457-9.

22. Jiang, H. & Powers, T. R. Curvature-Driven Lipid Sorting in a Membrane Tubule. *Phys. Rev. Lett.* **101**, 018103 (2008). DOI 10.1103/PhysRevLett.101.018103.

23. Singh, P., Mahata, P., Baumgart, T. & Das, S. L. Curvature sorting of proteins on a cylindrical lipid membrane tether connected to a reservoir. *Phys. Rev. E* **85**, 051906 (2012). DOI 10.1103/PhysRevE.85.051906.

24. McDargh, Z. A., Vázquez-Montejo, P., Guven, J. & Deserno, M. Constriction by Dynamin: Elasticity versus Adhesion. *Biophys. J.* **111**, 2470–2480 (2016). DOI 10.1016/j.bpj.2016.10.019.

25. Helfrich, W. Elastic properties of lipid bilayers: Theory and possible experiments. *Zeitschrift fur Naturforschung. Teil C* **28**, 693–703 (1973).

26. Ou-Yang, Z.-C., Liu, J.-X. & Xie, Y.-Z. *Geometric Methods in the Elastic Theory of Membranes in Liquid Crystal Phases* (World Scientific, Singapore, 1999).

27. Steigmann, D., Baesu, E., Rudd, R. E., Belak, J. & McElfresh, M. On the variational theory of cell-membrane equilibria. *Interfaces Free. Boundaries* **5**, 357–366 (2003).

28. Kreyszig, E. *Differential Geometry* (Dover Publications, New York, 1991), 1st edition edn.

29. Frankel, T. *The Geometry of Physics: An Introduction* (Cambridge University Press, Cambridge ; New York, 2011), 3 edition edn.

30. Walani, N., Torres, J. & Agrawal, A. Endocytic proteins drive vesicle growth via instability in high membrane tension environment. *Proc. Natl. Acad. Sci.* **112**, E1423–E1432 (2015). DOI 10.1073/pnas.1418491112.

31. Hassinger, J. E., Oster, G., Drubin, D. G. & Rangamani, P. Design principles for robust vesiculation in clathrin-mediated endocytosis. *Proc. Natl. Acad. Sci.* 201617705 (2017). DOI 10.1073/pnas.1617705114.

32. Rawicz, W., Olbrich, K. C., McIntosh, T., Needham, D. & Evans, E. Effect of Chain Length and Unsaturation on Elasticity of Lipid Bilayers. *Biophys. J.* **79**, 328–339 (2000). DOI 10.1016/S0006-3495(00)76295-3.

33. Steigmann, D. J. Fluid Films with Curvature Elasticity. *Arch. for Ration. Mech. Analysis* **150**, 127–152 (1999). DOI 10.1007/s002050050183.

34. Agrawal, A. & Steigmann, D. J. A model for surface diffusion of trans-membrane proteins on lipid bilayers. *Zeitschrift für angewandte Math. und Physik* **62**, 549 (2011). DOI 10.1007/s00033-011-0132-5.

35. Osserman, R. *A Survey of Minimal Surfaces* (Dover Publications, Mineola, New York, 1996). Google-Books-ID: WHN444vBvioC.

36. Torquato, S. & Donev, A. Minimal surfaces and multifunctionality. *Proc. Royal Soc. Lond. A: Math. Phys. Eng. Sci.* **460**, 1849–1856 (2004). DOI 10.1098/rspa.2003.1269.

37. Powers, T. R., Huber, G. & Goldstein, R. E. Fluid-membrane tethers: Minimal surfaces and elastic boundary layers. *Phys. Rev. E* **65**, 041901 (2002). DOI 10.1103/PhysRevE.65.041901.

38. Goldstein, R. E., Moffatt, H. K., Pesci, A. I. & Ricca, R. L. Soap-film Möbius strip changes topology with a twist singularity. *Proc. Natl. Acad. Sci.* **107**, 21979–21984 (2010). DOI 10.1073/pnas.1015997107.

39. Snapp, E. L. *et al.* Formation of stacked ER cisternae by low affinity protein interactions. *J. cell biology* **163**, 257–269 (2003). DOI 10.1083/jcb.200306020.

40. Terasaki, M. *et al.* Stacked Endoplasmic Reticulum Sheets Are Connected by Helicoidal Membrane Motifs. *Cell* **154**, 285–296 (2013). DOI 10.1016/j.cell.2013.06.031.

41. Bahmani, F., Christenson, J. & Rangamani, P. Analysis of lipid flow on minimal surfaces. *Continuum Mech. Thermodyn.* **28**, 503–513 (2015). DOI 10.1007/s00161-015-0458-x.

42. Rangamani, P., Agrawal, A., Mandadapu, K. K., Oster, G. & Steigmann, D. J. Interaction between surface shape and intra-surface viscous flow on lipid membranes. *Biomech. Model. Mechanobiol.* **12**, 833–845 (2013). DOI 10.1007/s10237-012-0447-y.

43. Agrawal, A. & Steigmann, D. J. Boundary-value problems in the theory of lipid membranes. *Continuum Mech. Thermodyn.* **21**, 57–82 (2009). DOI 10.1007/s00161-009-0102-8.

44. Hu, M., Briguglio, J. J. & Deserno, M. Determining the Gaussian Curvature Modulus of Lipid Membranes in Simulations. *Biophys. J.* **102**, 1403–1410 (2012). DOI 10.1016/j.bpj.2012.02.013.

45. Boulant, S., Kural, C., Zeeh, J.-C., Ubelmann, F. & Kirchhausen, T. Actin dynamics counteract membrane tension during clathrin-mediated endocytosis. *Nat. Cell Biol.* **13**, 1124–1131 (2011). DOI 10.1038/ncb2307.

46. Derényi, I., Jülicher, F. & Prost, J. Formation and Interaction of Membrane Tubes. *Phys. Rev. Lett.* **88**, 238101 (2002). DOI 10.1103/PhysRevLett.88.238101.

47. Liu, J., Kaksonen, M., Drubin, D. G. & Oster, G. Endocytic vesicle scission by lipid phase boundary forces. *Proc. Natl. Acad. Sci.* **103**, 10277–10282 (2006).

48. Beck, R. *et al.* Coatomer and dimeric ADP ribosylation factor 1 promote distinct steps in membrane scission. *The J. Cell Biol.* **194**, 765–777 (2011). DOI 10.1083/jcb.201011027.

49. Boucrot, E. *et al.* Membrane Fission Is Promoted by Insertion of Amphipathic Helices and Is Restricted by Crescent BAR Domains. *Cell* **149**, 124–136 (2012). DOI 10.1016/j.cell.2012.01.047.

50. Rossman, J. S., Jing, X., Leser, G. P. & Lamb, R. A. Influenza Virus M2 Protein Mediates ESCRT-Independent Membrane Scission. *Cell* **142**, 902–913 (2010). DOI 10.1016/j.cell.2010.08.029.

51. Saikia, K., Sravani, Y. D., Ramakrishnan, V. & Chaudhary, N. Highly potent antimicrobial peptides from N-terminal membrane-binding region of E. coli MreB. *Sci. Reports* **7**, 42994 (2017). DOI 10.1038/srep42994.

52. Kooijman, E. E. *et al.* Spontaneous curvature of phosphatidic acid and lysophosphatidic acid. *Biochem.* **44**, 2097–2102 (2005).

53. Churchward, M. A. *et al.* Specific Lipids Supply Critical Negative Spontaneous Curvature—An Essential Component of Native Ca2+-Triggered Membrane Fusion. *Biophys. J.* **94**, 3976–3986 (2008). DOI 10.1529/biophysj.107.123984.

54. Schmidt, N. W. *et al.* Criterion for Amino Acid Composition of Defensins and Antimicrobial Peptides Based on Geometry of Membrane Destabilization. *J. Am. Chem. Soc.* **133**, 6720–6727 (2011). DOI 10.1021/ja200079a.

55. Van Meer, G., Voelker, D. R. & Feigenson, G. W. Membrane lipids: Where they are and how they behave. *Nat. reviews molecular cell biology* **9**, 112–124 (2008).

56. Frolov, V. A., Lizunov, V. A., Dunina-Barkovskaya, A. Y., Samsonov, A. V. & Zimmerberg, J. Shape bistability of a membrane neck: A toggle switch to control vesicle content release. *Proc. Natl. Acad. Sci.* **100**, 8698–8703 (2003). DOI 10.1073/pnas.1432962100.

57. Irajizad, E., Walani, N., Veatch, S. L., Liu, A. P. & Agrawal, A. Clathrin polymerization exhibits high mechano-geometric sensitivity. *Soft Matter* **13**, 1455–1462 (2017). DOI 10.1039/C6SM02623K.

58. Isenberg, C. *The Science of Soap Films and Soap Bubbles* (Dover Publications, New York, 1978). Google-Books-ID: PdsVME_LXTYC.

Acknowledgments

This work was supported in part by AFOSR FA9550-15-1-0124 and NSF PHY-1505017 awards to P.R. The authors thank Jasmine Nirody and Miriam Bell for critical reading.

Author Contributions

All authors developed the model, discussed the results, and wrote the paper. M.C. performed the simulations.

Competing Financial Interests

The authors declare no competing financial interests.